

Supplementary Materials for **Polarization recovery through scattering media**

Hilton B. de Aguiar, Sylvain Gigan, Sophie Brasselet

Published 1 September 2017, *Sci. Adv.* **3**, e1600743 (2017)

DOI: 10.1126/sciadv.1600743

This PDF file includes:

- section S1. Polarization state evaluation
- section S2. Vectorial transmission matrix analysis under broadband conditions
- section S3. Comparison with a monochromatic transmission matrix
- section S4. Time-of-flight results
- section S5. Exclusion of ballistic hypothesis
- section S6. Model for nonanalyzed SHG response
- section S7. On the role of bandwidth
- section S8. Discussion on theoretical models
- fig. S1. Polarization state evaluation of the refocused light for the brain specimen.
- fig. S2. Polarization state evaluation of the refocused light.
- fig. S3. Effect of transmission matrix interelement coupling on cross-correlation.
- fig. S4. Cross-correlation between various transmission matrices.
- fig. S5. Comparison of different transmission matrix acquisition methods.
- fig. S6. Time-of-flight results.
- fig. S7. Size of the refocus, enhancement, contrast, and ballistic contribution versus optical thickness.
- fig. S8. Bandwidth results.
- References (44–56)

section S1. Polarization state evaluation

We performed two types of experiments to assess the quality of polarization when performing polarized refocussing under broadband conditions, respectively addressing the quality of the polarization conservation and the quality of the polarization state at the focus. Figure S1 addresses the first point, showing the refocus intensity dependence to a rotation of the linear incident polarization. Without any analyzer at the exit of the medium (here a 1 mm-thick mouse brain tissue) (fig. S1, left), the intensity hardly changes, which means that the energy is kept constant even though the incident polarization is different from the one used for refocussing. When using an analyzer before the detector (fig. S1, right), complete extinction can be detected for an input polarization perpendicular to the analyzer direction, showing that the produced polarization dependence is not the result of a depolarized process, but rather from polarization. Figure S1 (right) is fitted by a Malus law generally used for pure polarization propagation.

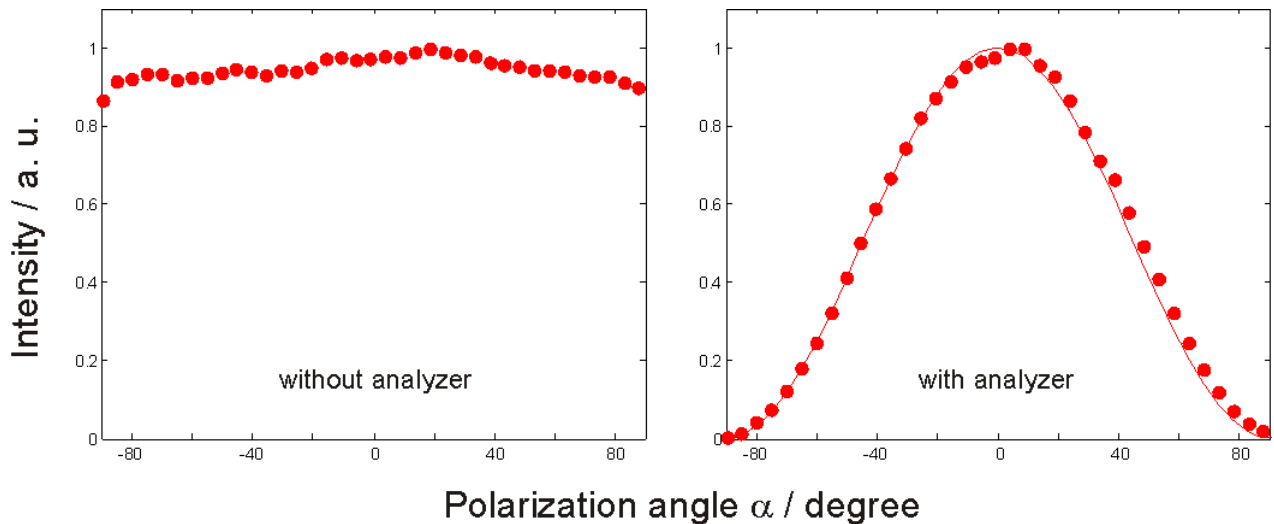


fig. S1. Polarization state evaluation of the refocused light for the brain specimen. (left) Intensity measurement of the refocus upon rotation of the input electric field. (right) Same, but with an analyzer placed in the output detection. The line is a plot of $(\cos \alpha + A)$, where A is a constant due to speckle background and α is the input polarization state angle.

Figure S2 shows how linear is the output polarization obtained after refocussing. We analyzed the polarization state by using the well known quarter-waveplate method (45), which consists in rotating a quarter-waveplate before a fixed polarizer, and interpreting the obtained modulation to deduce the complete set of Stokes parameters from the obtained polarization. When analyzed without any scattering medium, the polarization is seen to be almost purely linear along the horizontal axis with Stokes parameters $[S_0, S_1, S_2, S_3] = [1, 0.98, -0.16, -0.06]$, which leads to a degree of polarization of $DOP = \frac{\sqrt{S_1^2 + S_2^2 + S_3^2}}{S_0} = 0.97$. Adding the scattering medium ($L/l_t \approx 6$) leads to a response with new Stokes parameters, respectively $[1, 0.94, -0.07, 0]$ and $[1, -0.94, 0.02, 0.07]$ for the parallel and perpendicular input polarizations. In both cases, a degree of polarization of 94% is obtained, which is very high considering the thick sample measured, and the initial depolarization obtained from the averaged speckle before refocussing. To stress the correlation with the input state, fig. S2 (left, continuous lines) shows the response using Stokes parameters without the scattering medium (the original input polarization state). In comparison, the background surrounding speckle (which is subtracted in the refocus analysis) is 10 times lower in averaged intensity and has very different polarization responses depending on the speckle grain measured (fig. S2, right). The individual polarization responses shown in fig. S2 (right) are characteristic of various polarization states from linear to elliptic, with a high degree of *depolarization*, as shown by the low contrasts of the polarization responses (low modulation amplitude).

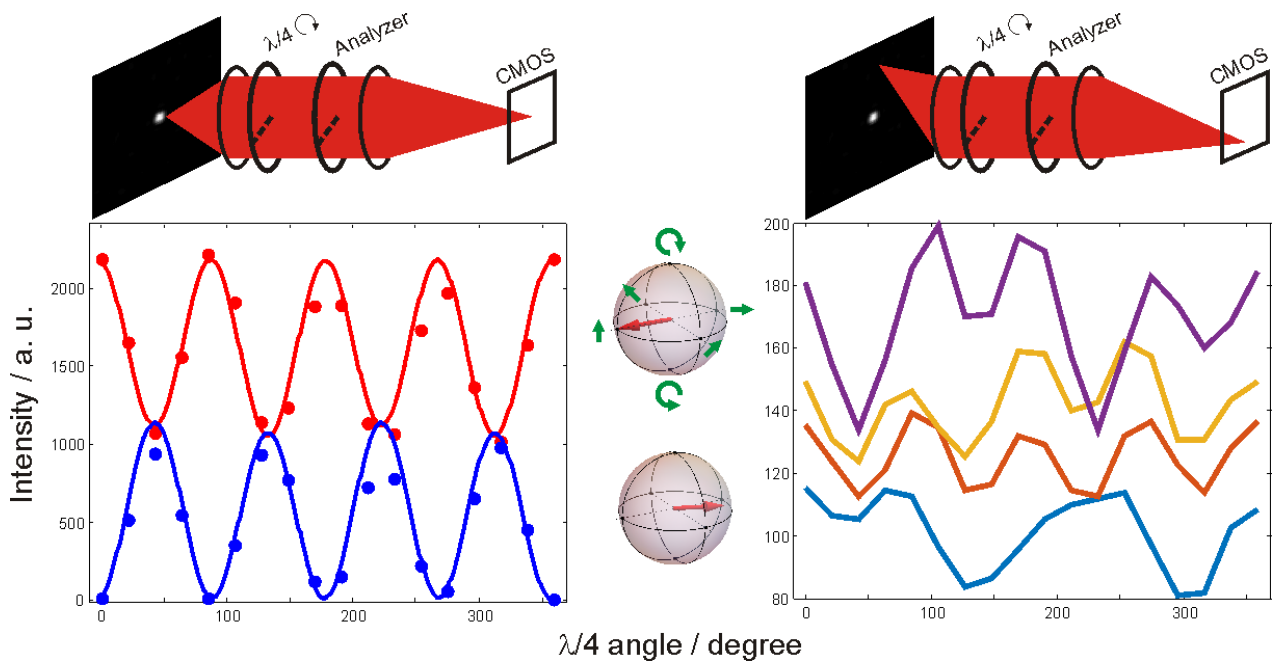


fig. S2. Polarization state evaluation of the refocused light. Left: (markers) response obtained from the quarter-waveplate rotation (scheme shown on the top) at the refocus position, corrected by background subtraction. Red: input vertical polarization. Blue: input horizontal polarization. The continuous line is a plot (model) using the corresponding Stokes parameters without the scattering medium (45). Middle: Poincaré sphere representation of the Stokes parameters. Right: different responses obtained from different regions in the background speckle around the refocus point. The intensity is on average 10 times lower than at the refocus. The medium used for this experiment is $L/l_t \approx 6$. The plots have been offset for clarity.

section S2. Vectorial transmission matrix analysis in broadband conditions

A. Reducing correlations in the vectorial transmission matrix

Correlations are present among the elements of the scalar transmission matrix (44, 46). These correlations can be intrinsic to scattering phenomena (coherent backscattering) (46) or induced experimentally (input or output inter-element coupling) (44, 46). To remove this inter-element coupling, we obtained filtered transmission matrices from the original ones by considering only every second (fig. S3, left panel), fourth (fig. S3, middle panel) and eighth output channel (fig. S3, right panel) for the cross correlation analysis. As it can be seen in fig. S3, some inter-element coupling arise from oversampling the output channels (oversampled speckle grains) and is evidenced by the presence of multiple peaks in the cross-correlation (fig. S3, left panel). A second conclusion drawn from fig. S3 is that no considerable coupling in the input channels is present, since no extra peaks are observed along the input channels in the cross correlation. Therefore, we only considered removal of inter-element output channels relevant for the analysis.

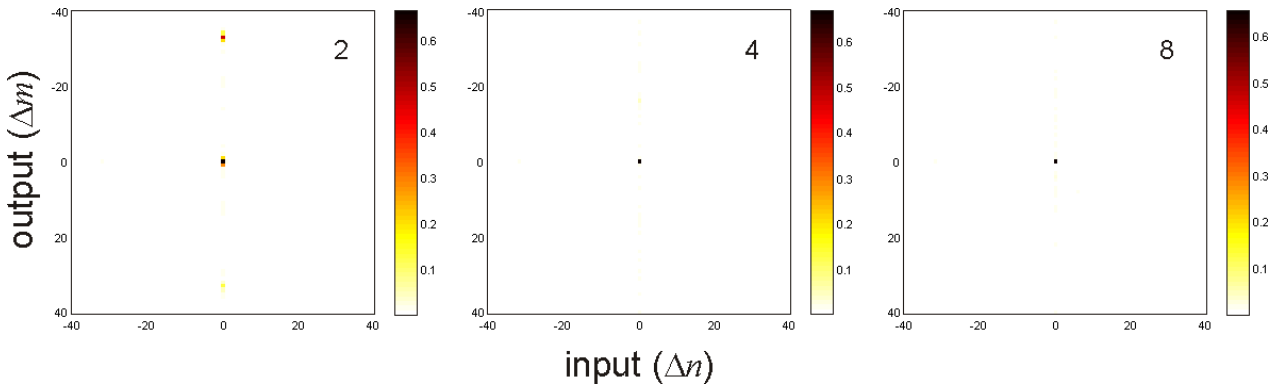


fig. S3. Effect of transmission matrix interelement coupling on cross-correlation (between t^{xx} and t^{yy}). The cross-correlation was performed using filtered transmission matrix taking every second (left panel), fourth (middle panel) and eighth (right panel) output channel from the original transmission matrices. The region of interest is within lags where clear peaks can be seen.

B. Correlations between the polarization-related part of the vectorial transmission matrix

Figure S4 shows cross correlation between sub-parts of the vectorial transmission matrices. As in section 2.A, we use the filtered transmission matrices for the analysis. The normalization of the cross correlation is with respect to the amplitude autocorrelation of one of the matrices considered.

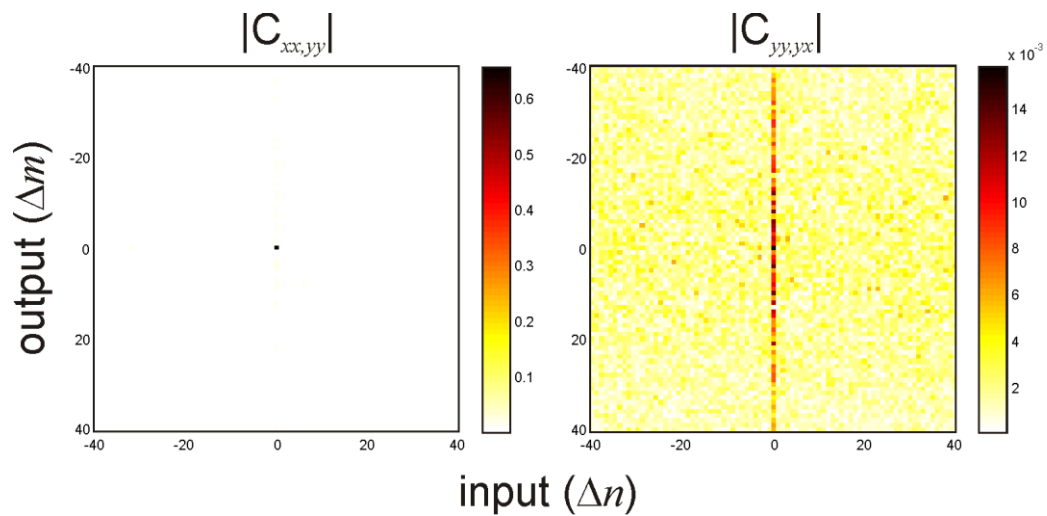


fig. S4. Cross-correlation between various transmission matrices t^{ij} as indicated in the top of each panel.

section S3. Comparison with a monochromatic transmission matrix

Figure S5 shows results comparing the broadband transmission matrix with a monochromatic transmission matrix measured using a CW laser source (1070 nm, IPG Photonics). The scattering medium is the very same for both methods. However, because of the different wavelength used, the optical thickness differ by $\approx 2\%$.

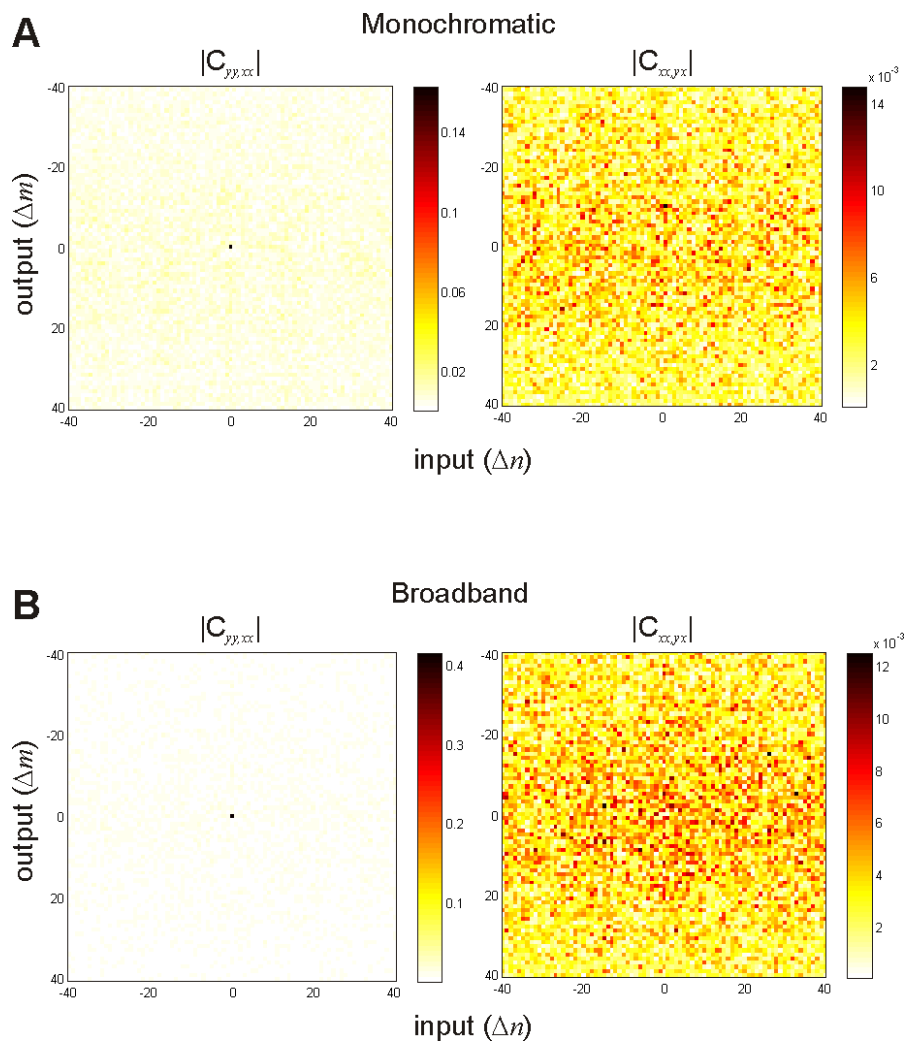


fig. S5. Comparison of different transmission matrix acquisition methods acquired using the very same medium. Cross-correlations of the monochromatic (A) and broadband (B) transmission matrices are performed as explained in section 2.A.

section S4. Time-of-flight results

Here, we infer a microscopic explanation of the polarization recovery effect. Figure S6 presents time-of-flight results using the setup thoroughly described in ref. (47). Basically, it consists of low-pass filtering a cross-correlation measurement of the speckle grain with an ultrashort external pulse. The two curves are for averages over many speckle grains (unshaped) and refocus realizations (shaped). Note that for a fair comparison, and also to stress the inherent selection of polarization-preserving photons, the two curves are for a sampling of the parallel polarization state. While the unshaped case shows a clear long pathlength, the shaped refocus with a broadband source inherently selects short pathlength photons (note the suppression of the long pathlengths). This explains partially the polarization recovery effect, since the short pathlength photons have on average undergone less scattering events. Shaping with a monochromatic source (19, 20) or broadband shaping using a strongly scattering thin medium (we have tested for TiO_2 thin films with $DOLP \approx 0.1$) leads to absence of polarization recovery.

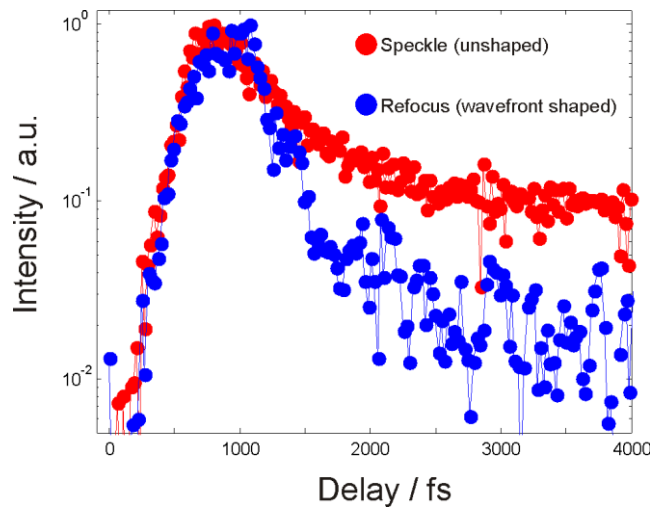


fig. S6. Time-of-flight results for and unshaped speckle (red, averaged over 400 random points in the field-of-view) and at the refocus position after shaping (blue, averaged over 4 refocus realization). The plots are normalized to their maximum intensity in order to highlight the suppression of long pathlength photons. Note that neither spectral degree of freedoms are shaped, nor nonlinear optical process were used for achieving this result.

section S5. Exclusion of ballistic hypothesis

In this section, we discuss extensively the possible contribution of ballistic light, that is, un-scattered light. We show that our observations depart drastically from what would be expected based on ballistic focusing.

Figure S7A presents evaluation of the refocus size versus optical thickness L/l_t . For sample thickness comparable to l_t , even though l_t/l_s scattering events have happened, the behavior is still reminiscent of un-scattered light. That is, light still preserves a high-degree of memory in respect to the original wavefront forming a focus that is dictated by the incoming numerical aperture (NA) (26, 48, 49). As the optical thickness increases, the relative contribution of this memory-preserving photons is decreased and more multiply scattered light increases its effective "NA" (spatial frequency bandwidth) thus leading to a smaller refocus. These two extremes are schematically pictured in the inset of the fig. S7. The two dashed lines are theoretical values of the expected refocus size. The low- L/l_t is dictated by the NA of the focusing lens behind the medium. The high- L/l_t is dictated by the speckle grain size ($\lambda/2$) convoluted with the detection NA.

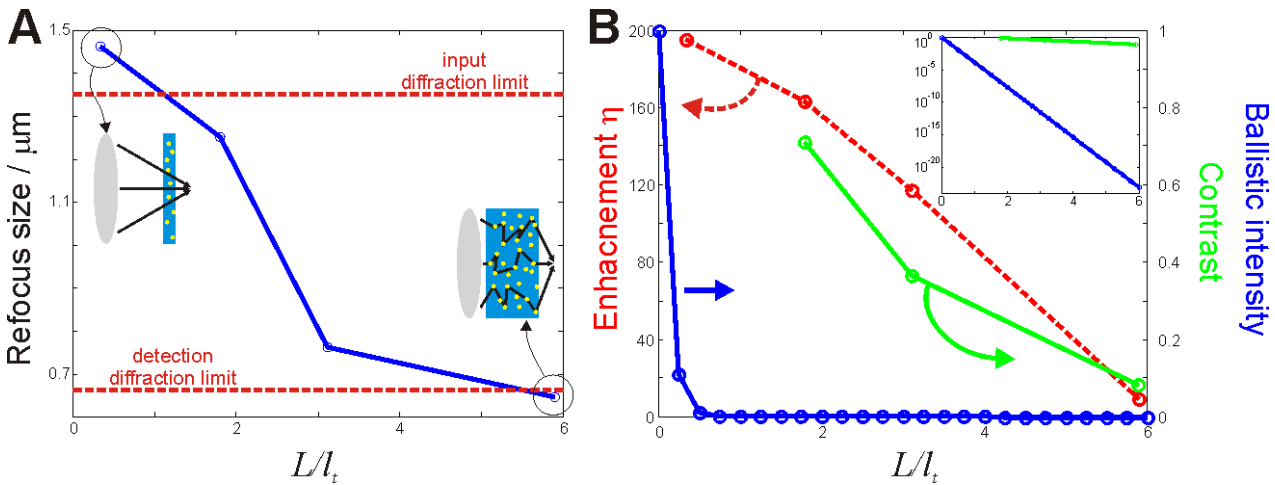


fig. S7. Size of the refocus, enhancement, contrast, and ballistic contribution versus optical thickness. (A) Size of the refocus vs. optical thickness (continuous lines). The inset are illustrations of the most dominant contribution to the refocus position. Read text for further explanation. **(B)** Enhancement, contrast (experimental) and ballistic contribution (simulation) vs. optical thickness.

Further evidence is provided by showing that the energy contribution to the refocus is mostly due to multiply scattered light. Figure S7B shows the enhancements η and contrast C vs. L/l_t , both related through $\eta = C \frac{\pi}{4} N_{SLM}$, where N_{SLM} is the number of controlled SLM segments. C is related to the ratio between the medium spectral bandwidth to the source bandwidth (16, 17, 42, 47). Due to speckle temporal decorrelation of the medium used, we have an overall η that is below the theoretical value. Nevertheless, fig. 7B shows that the two quantities remarkably follow the same trend, demonstrating that the energy contribution to the refocus is mostly due to multiply-scattered diffuse light. To stress this point better, we further model in fig. S7B the intensity expected of the ballistic contribution (through the well-known Beer-Lambert law). As it is clear from this plot, the relative contribution of ballistic photons is of the order of e^{-49} a value that is difficult to detect with current table-top apparatus within minutes.

All in all, we can conclude that ballistic light contribution is negligible to the refocus position. Furthermore, we calculated the optical thickness using an analysis based on diffusion theory (31), obtaining values that are in the same order-of-magnitude as directly measured, indicating that the diffusive regime is fully developed.

section S6. Model for nonanalyzed SHG response

For a thorough analysis of polarization-resolved nonlinear microscopy the reader is referred to ref. (1).

The SHG intensity $I_{teo}(\alpha) = |P_x^{(2)}(\alpha)|^2 + |P_y^{(2)}(\alpha)|^2$ (measured with an input polarization state angle α) depends on the induced second order polarization $P_i^{(2)}(\alpha) = \sum_{jk} \chi_{ijk,lab}^{(2)}(\phi) E_j(\alpha) E_k(\alpha)$, with $\chi_{ijk,lab}^{(2)}$ the nonlinear SHG tensor expressed in the laboratory frame. In order to relate this measurement to the properties of collagen (molecular order and mean orientation), we need to relate this laboratory frame tensor to the collagen fiber frame $\chi_{abc}^{(2)}$ tensor, (a, b, c) being the axes of the collagen fiber frame with c its long axis. The fiber is supposed to be of cylindrical symmetry (rigorously of C_6 symmetry along the c axis) and aligned in the sample plane with an angle ϕ relative to the horizontal sample axis. Therefore, $\chi_{ijk,lab}^{(2)}(\phi)$ only depends on the orientation ϕ and on the microscopic collagen tensor characterized by two coefficients, $\chi_{ccc}^{(2)}$ and $\chi_{aac}^{(2)} = \chi_{bbc}^{(2)} = \chi_{caa}^{(2)} = \chi_{cbb}^{(2)}$. The exact expression of this dependence is obtained by rotation of the microscopic tensor in the laboratory frame, as described elsewhere (1). The obtained polarization response thus solely depends on ϕ and the ratio $R = \chi_{ccc}^{(2)} / \chi_{aac}^{(2)}$. R is empirically related to molecular order in collagen fibers (50–52) and is obtained by minimizing $\sum_i |I_{exp}(\alpha_i) - I_{teo}(\alpha_i)|^2$ where $I_{exp}(\alpha)$ is the total SHG intensity ($I_x + I_y$) measured with an input polarization state angle α . The collagen order value obtained ($R=1.4$) is in excellent agreement with previous observations (50, 51). The mean orientation ϕ of the obtained collagen molecules with respect to the laboratory frame is found to be independent on the obtained R value, as expected. In general the orientation ϕ is found to be along the visualized collagen fibers on the image, except in thick samples where birefringence can influence the obtained orientation (52). In such cases, this effect needs to be accounted for in order to properly interpret the data.

section S7. On the role of bandwidth

According to our observations and model, there are two features to observe polarization recovery: differential contrast between the output speckles for the two polarization states, and a medium speckle spectral correlation bandwidth $\delta\omega$ smaller than the source bandwidth $\Delta\omega$ ($\delta\omega < \Delta\omega$). Here, we present experiments performed on similar scattering system ($DOLP = 0.3$, $L/l_t \sim 6$) as in the main manuscript, however using a different source of intermediary bandwidth (picosecond pulses) fulfilling $\delta\omega < \Delta\omega$. We estimate $\delta\omega$ from the pulse contrast measured with a broadband femtosecond source with a known bandwidth $\Delta\omega$ (as in (31)). The contrast $C = 0.12$ measured with the broadband source corresponds to 70 independent spectral speckle modes $N_\omega = \Delta\omega/\delta\omega$ ($C = 1/\sqrt{N_\omega}$), or a medium with $\delta\omega \approx 90$ pm [or alternatively 11 ps long pulse leaving the medium (47)].

Figure S8A shows an overview of the measured differential contrast ($C_{xx} - C_{yx}$), normalized by the non-analyzed contrast C , for various laser sources bandwidths. A value of 1 means that the modulation amplitude in the interferometric measurement is dominated by xx polarization combination. Accordingly, we expect polarization recovery for the picosecond source. Indeed, fig. S8B shows that refocusing with picosecond pulses is robust upon a change in the input polarization state. This indicates that polarization recovery is achieved in agreement with the model.

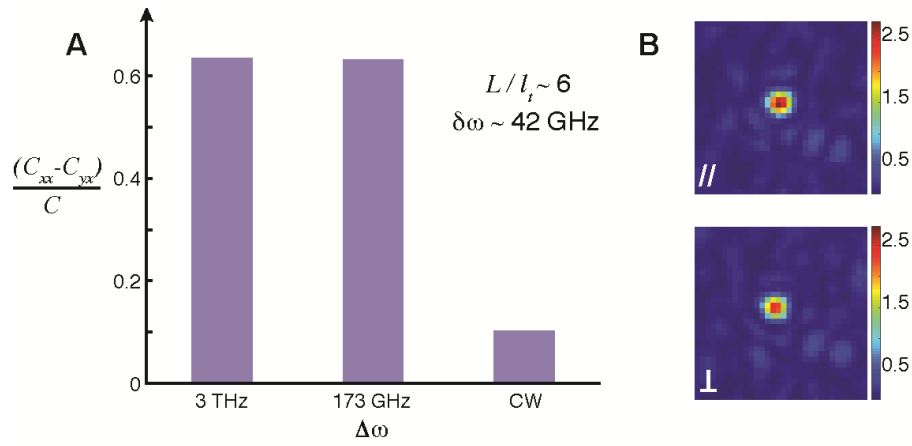


fig. S8. Bandwidth results. (A) Normalized differential contrast of the output speckles for various laser sources bandwidth $\Delta\omega$. (B) The same experiment as shown in the manuscript, however using a picosecond source ($\Delta\omega = 173$ GHz). The robustness of the refocus against a change in the input polarization state demonstrates polarization recovery.

section S8. Discussion on theoretical models

Here, we review current models to describe the vectorial propagation of fields and the challenges on modelling complex media. Recent studies have revealed that much remains to be explored and understood on the relation between the microscopic structure of scattering media and the polarization properties of scattered fields. A fortiori, modelling the effect of wavefront shaping is much less developed since it requires approaches that do not derive averaged properties of scattered fields. In the context of this work, one would need to include the broadband nature of the illumination, and also consider anisotropic scattering media (e.g. that exhibit short range correlations).

Theoretically describing the propagation of polarized light in disordered media is a challenging task, and we briefly overview the main achievements. Radiative transfer equation has been extended to a vectorial context for describing Stokes parameters (53). This allowed to define degree of depolarization in complex media, however spatially averaged. Transfer matrix formalism combined with Monte Carlo simulations lead to a phenomenological definition of the distinct photon pathlengths distribution affecting polarization modes in anisotropic scattering media (54), successfully explaining the differences in the two output speckle contrast under broadband excitation conditions (55). Multiple scattering theory has been used to model polarized light propagation in uncorrelated (isotropic) media (32), and on media exhibiting short-range structural correlations (33). This formalism is however only developed in the monochromatic regime.

In all the works above, all results are either performed on very small idealized systems (a few tens to a few hundreds of scatterers), or derived based on a statistical description of the disorder, never by solving propagation equations on a single realization. Therefore, despite remarkably advancing microscopic understanding of light propagation in complex media, such models are not suited to the wavefront shaping experiments. The key point is that a wavefront shaping experiment is deterministic, thus approaches that involve averaged quantities (field and field correlation) are not directly transferable for describing a wavefront shaping experiment. Conversely, finite-difference time-domain can be used to construct the transmission matrix of a medium (35). However, so far it only addresses 2D systems

under scalar approximation, and for monochromatic fields. Other less heavy computational methods are in continuous development (36, 37, 38) with the main goal of microscopically understanding the outcome of the wavefront shaping experiment, with a good success (34, 56). Nevertheless, these models are scalar, do not consider anisotropic scattering media, and are in the monochromatic regime (except (37) that considers a broadband source).

Summarizing, our results show an effect that occurs specifically in broadband polarized wavefront shaping of anisotropic scattering media. Therefore, in order to understand its microscopic origins, we need new specificities for the regime observed, in which the waves self-interferometry takes place deterministically. In particular, our findings support direct conclusions that the pathlength distribution contributing to the optimization process is affected by; (i) a reduction of interference visibility for long pathlengths; (ii) and different characteristics for co- and cross-polarized modes in the medium upon wavefront shaping.